HHS Public Access

Author manuscript

*ACS Biomater Sci Eng*. Author manuscript; available in PMC 2020 March 04.

Published in final edited form as:

*ACS Biomater Sci Eng*. 2019 December 9; 5(12): 6570–6580. doi:10.1021/acsbiomaterials.9b00947.

# Development and Evaluation of Paclitaxel-Loaded Aerosol Nanocomposite Microparticles and Their Efficacy Against Air-Grown Lung Cancer Tumor Spheroids

**Elisa A. Torrico Guzmán**[1], **Qihua Sun**[1], **Samantha A. Meenach**[1,2]

[1]University of Rhode Island, College of Engineering, Department of Chemical Engineering, 360 Fascitelli Center of Advanced Engineering, 2 Upper College Road, Kingston, RI 02881, USA

[2]University of Rhode Island, College of Pharmacy, Department of Biomedical and Pharmaceutical Sciences, Avedisian Hall, 7 Greenhouse Road, Kingston, RI 02881, USA

## Abstract

Paclitaxel (as intravenous Taxol) is one of the most applied chemotherapeutics used for the treatment of lung cancer. This project involves the development of a dry powder nanocomposite microparticle (nCmP) aerosol containing PTX-loaded nanoparticles (NP) to be delivered via a dry powder inhaler to the lungs for the treatment of non-small cell lung cancer (NSCLC). Nanoparticles were formulated by a single emulsion and solvent evaporation method, producing smooth, neutral PTX NP of approximately 200 nm in size. PTX nCmP were obtained via spray drying PTX NP with mannitol, producing amorphous wrinkled particles that demonstrated optimal aerosol deposition for *in vitro* pulmonary delivery. Free PTX, PTX NP, and PTX nCmP were evaluated *in vitro* in both 2D monolayers and 3D multicellular spheroids (MCS). PTX NP enhanced cytotoxicity when compared to pure drug in the 2D evaluation. However, on a liquid culture 3D tumor spheroid model, PTX NP and pure PTX showed similar efficacy in growth inhibition of MCS. The PTX nCmP formulation had a comparable cytotoxicity impact on MCS compared with free PTX. Finally, PTX nCmP were evaluated in an air-grown 3D MCS platform that mimics the pulmonary environment, representing a new model for the assessment of dry powder formulations.

## Graphical Abstract

***Corresponding Author***: Samantha A. Meenach, University of Rhode Island, 309 Fascitelli Center of Advanced Engineering, 2 Upper College Road, Kingston, RI 02881, USA. smeenach@uri.edu.

SUPPORTING INFORMATION

Supporting information include: Schematic of the synthesis of acetalated dextran (Ac-Dex); Representative $^{+}$H-NMR spectrum of acetalated dextran (Ac-Dex) degradation products; Table of the $^{+}$H-NMR results; and Analysis of the diameter of A549 multicellular spheroids (MCS) grown in an 3D air interface cell culture (AIC) platform over time.

AUTHOR DISCLOSURE STATEMENT

No conflict of interest exists.

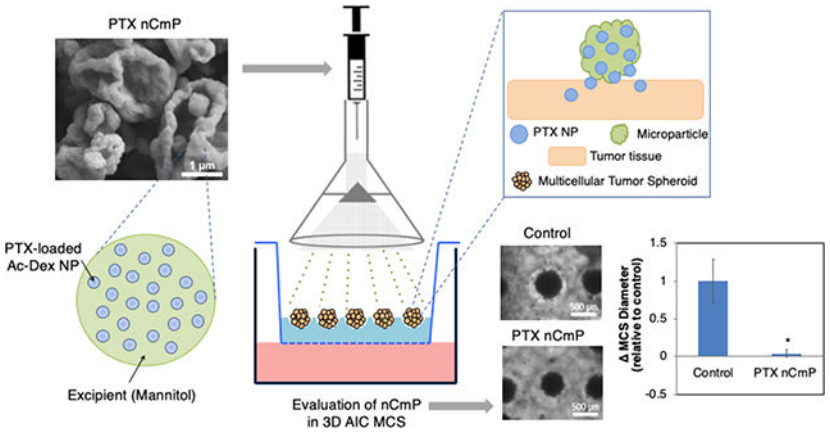


**Keywords**

Paclitaxel nanocomposite microparticles; lung cancer; pulmonary delivery; multicellular tumor spheroids; air-interface cell culture

## 1. INTRODUCTION

Lung & bronchus cancer is the leading cause of cancer-related deaths in the United States, with an estimated of 228,150 new cases anticipated for 2019 and a mortality of 390 deaths per day. The 5-year relative survival rate of a patient diagnosed with lung cancer is 19%.[1] Chemotherapy has been extensively used in the treatment of lung cancer, with the use of potent drugs delivered intravenously (I.V.). Such systemic delivery is often associated with high toxicity, high dosages, and low specificity. Pulmonary delivery has emerged as an attractive route of delivery of therapeutics to treat diseases such as lung cancer, as it can overcome limitations associated with I.V. delivery.[2] Aerosol therapeutics involve a non-invasive delivery system that can utilize lower doses of drug with fewer systemic side effects.[3–4]

Dry powder inhalers (DPIs) are often preferred over other aerosols devices as they can offer physical stability of formulations in solid form, are portable and easy to use, and can be applied to a wide variety of active ingredients and dosages.[5–6] While micron-sized particles (1 – 5 μm) can be easily delivered to the deep airways, they are easily removed from the airways via phagocytosis.[7] In turn, nanocarriers offer advantages such as the ability to penetrate physiological barriers, improved colloidal stability of hydrophobic drugs, and sustained release of therapeutics, which can reduce dosing frequency.[8]

Particle deposition in the lungs following aerosolization is dependent on their size, morphology, and density, among other factors.[9] Overall, the aerosol performance of particles is determined by their aerodynamic diameter.[10] Larger particles are deposited in the airways by impaction and sedimentation, while smaller particles deposit by diffusion (Brownian motion).[11–12] The optimal particle size (aerodynamic diameter) for deep lung deposition has been established to be between 1 and 5 μm.[12] In this regard, NP deposition is limited because of their low inertia and high possibility of being exhaled. Micron-sized aggregates

of nanoparticles (i.e. nanocomposite microparticles) typically have enough mass to deposit effectively into the lungs. Once these particles deposit in the airways, they dissociate back into nanoparticles.[13–14] Studies reporting examples of inhalable dry powder formulations based on nanocomposite microparticles (nCmP) include tobramycin-loaded PLGA NP for bacterial infections,[15] poly(glycerol adipate-co-ω-pentadecalactone) NP loaded with a pneumococcal antigen for pneumonia vaccination,[16] POxylated polyurea dendrimer-based NP loaded with chemotherapeutics[17], and ibuprofen, a common anti-inflammatory drug.[18] nCmP can improve the delivery of drugs due to their ability to provide tunable lung deposition while delivering drug-loaded NP to the different regions in the lungs.[19]

Paclitaxel (PTX) is a microtubular stabilizer chemotherapeutic characterized by its high toxicity, low water solubility (~0.4 μg/ml), and need to use excipients in IV delivery.[20] The hydrophobicity of PTX limits its bioavailability, thus there has been significant work to develop PTX nanocarriers using polymeric micelles, liposomes, nanoemulsions, etc.[21] Chemotherapeutics are typically assessed in a 2-dimentional (2D) monolayer cell platform. However, this platform does not accurately represent complex tumor morphology, nor translate into similar results *in vivo*.[22] This misrepresentation can be due to the lack of dense extracellular matrix produced[23] and the lack of cell-particle interactions observed in tumors.[24–25]

Cancer cells tend to form solid tumors that are known to have hypoxic cells and a necrotic core, which often results in high resistance to treatment. Another reason for the failure of cancer treatments is low drug concentration in tumors due to transport and diffusion limitations.[26] Various techniques have been explored to fabricate *in vitro* multicellular spheroids (MCS),[27–30] that at sizes over 200 μm, develop an outer proliferating region, an inner quiescent region, and a hypoxic necrotic core, that can represent *in vitro* tumors.[31–33] 3D MCS can mimic tumor features such as spatial architecture, cell-cell signaling, physiological responses, gene expression patters, and drug resistance mechanisms.[34–35]

On this project we developed and characterized dry powder aerosol PTX nanocomposite microparticles for their potential in the treatment of lung cancer. PTX was encapsulated in acetalated dextran (Ac-Dex), a biodegradable, tunable polymer derived from dextran[36] via a single emulsion/solvent evaporation technique to produce PTX-loaded nanoparticles (PTX NP). These NP were then spray dried with mannitol to form nanocomposite microparticles that were characterized for lung deposition using a Next Generation Impactor (NGI). The impact of the PTX NP formulation on cancer cells was evaluated in a liquid covered culture (LCC) 2D cell monolayer followed by evaluation in LCC 3D MCS for NP, and PTX nCmp in air-interface culture (AIC) 3D MCS. The described 3D AIC platform may aid in the early evaluation of aerosol formulations in a more accurate and representative manner.

## 2. MATERIALS AND METHODS

### 2.1 Materials

Dextran from Leuconostic mesenteroides (MW 9,000–11,000), pyridinium p-toluenesulfonate (PPTS, 98%), anhydrous dimethyl sulfoxide (DMSO, ≥ 99.9%), 2-methoxypropene (2-MOP, 97%), triethylamine (TEA, ≥ 99%), deuterium chloride (DCl, 35

wt% in $D_2O$, 99% atom D), dichloromethane (DCM, > 99.8%), anhydrous sodium acetate, D-mannitol (≥ 98%), Triton™ X-100, bisBenzimide H 33342 trihydrochloride (Hoechst 33342), methanol (HPLC grade, ≥ 99.9%), and acetic acid (≥ 99%) were obtained from Sigma-Aldrich (Natick, MA, USA). Deuterium oxide ($D_2O$, 99.8% atom D), poly(vinyl alcohol) (PVA, 88% hydrolyzed, average MW 22,000), and curcumin (CUR, > 98%) were obtained from Acros Organics (Geel, Belgium). Formic acid (FA, ≥ 99.5%), glycine (≥ 98.5%), and Hydranal™ Coulomat AG Honeywell were obtained from Fisher Scientific (Somerville, NJ, USA). Phosphate buffered saline 10X (PBS) was obtained from Research Products International (RPI, Mount Prospect, IL, USA). Paclitaxel (> 99.5%) was purchased from LC Laboratories (Woburn, MA, USA). A549 human lung adenocarcinoma epithelial cells and NCl-H441 (H441) lung papillary adenocarcinoma epithelial cells were obtained from American Type Culture Collection (ATCC, Manassas, VA, USA). Fetal bovine serum (FBS) was obtained from Atlanta Biologics (Flowery Branch, GA, USA). RPMI 1640 1X with L-glutamine and 25 mM HEPES and collagen rat tail type I were obtained from Corning Inc. (Corning, NY, USA). Dulbecco's modified Eagle's medium (DMEM, 4.5 g/L d-glucose and L-glutamine), trypsin-EDTA (0.25%) phenol red, calcein AM, and ethidium homodimer-1 were obtained from Life Technologies™ (Carlsbad, CA, USA). Sodium pyruvate, penicillin streptomycin, and Fungizone were obtained from GE Health Life Sciences (Pittsburgh, PA, USA).

### 2.2 Synthesis of acetalated dextran (Ac-Dex)

The synthesis of acetalated dextran (Ac-Dex) was conducted as previously described.[37] Briefly, lyophilized dextran (1 g, MW 9–11,000) and the catalyst PPTS (25 mg) were dissolved in 10 mL of anhydrous DMSO under pure $N_2$ atmosphere. Dextran reacted with 5 mL of 2-MOP for 5 minutes and the reaction was quenched with 1 mL of TEA. The product was then precipitated dropwise in mildly stirring distilled water (300 mL, pH 9), vacuum filtered and thoroughly rinsed with extra distilled water. The product was frozen overnight and lyophilized (−50°C, 0.03 mBar) for 48 hours to remove residual water.

### 2.3 Nuclear magnetic resonance (NMR) analysis of acetalated dextran (Ac-Dex)

Conversion of hydroxyl groups (total acetal coverage) and the cyclic acetal coverage (CAC) were determined using $^1$H-NMR spectroscopy (Bruker 300 MHz NMR, MA, USA). In an NMR tube, 10 mg of Ac-Dex was suspended in 700 μL of $D_2O$, and then hydrolyzed with 30 μL of DCl. The hydrolysis of acyclic acetals produces methanol and acetone whereas cyclic acetals produce only acetone. The total acetal coverage and the CAC were determined after normalization of the methanol and acetone peaks in relation to the average of the dextran peaks. The normalization is associated with the number of protons detected on each molecule, and the results were expressed per 100 molecules of glucose. A more detailed description of the analysis of Ac-Dex may be found in the study by Broaders *et al.* (2009).[36]

### 2.4 Preparation of PTX-loaded Ac-Dex nanoparticles (PTX NP)

Paclitaxel-loaded nanoparticles (PTX NP) were prepared via a single emulsion and solvent evaporation method. 50 mg of PTX was dissolved in 1 mL of DMSO and 200 μL of this solution was added to 1800 μL of DCM. 1 mL of the PTX DCM solution was added to 95 mg of Ac-Dex (5 wt% initial PTX loading), forming the organic phase. 6 mL of 3% PVA in

PBS (aqueous phase) was added to the organic phase and sonicated (Q500 Sonicator, Qsonica, Newton, CT, USA) for 60 seconds with 1 second on/off pulse at an amplitude of 70% (100% amplitude = 120 μm). The resulting emulsion was transferred to a 40 mL spinning solution of 0.3% PVA in PBS and stirred for 4 hours to evaporate the organic solvent and stabilize the nanoparticles. The final solution was centrifuged at 12,000 rpm (19,802 g) and 4 °C for 20 minutes. The nanoparticles were washed twice with distilled water, frozen, and lyophilized (−50°C, 0.03 mBar) for 24 hours.

For the preparation of fluorescent NP for imaging (CUR NP), 1 mg of curcumin (CUR, fluorescent reagent) was dissolved in 1 ml DCM and added to 39 mg of Ac-Dex (organic phase) and made using the steps described above. Blank NP were made following the same procedures as CUR NP and PTX NP, excluding any dye or therapeutic.

### 2.5 Formulation of PTX nanocomposite microparticles (PTX nCmP) via spray drying

Paclitaxel nCmP were formulated with PTX NP and mannitol in an aqueous suspension using a Büchi B-290 spray dryer (Büchi Labortechnik, AG, Switzerland) in open mode. The ratio of PTX NP: mannitol was 80:20 (w/w) in DI water, which was suspended at a feed concentration of 0.5% (w/v). The spray dryer conditions were: 414 L/h dry $N_2$ flow rate, aspiration rate of 28 $m^3$/h, pump rate of 0.9 mL/min, inlet temperature of 90 °C, and nozzle cleaner rate of 4. The nCmP were collected in an amber glass vial and stored in desiccators at −20 °C.

### 2.6 Particle morphology and shape analysis via scanning electron microscopy (SEM)

The surface morphology and shape of the NP and nCmP were evaluated by scanning electron microscopy (SEM) with a Zeiss SIGMA VP Field Emission-SEM (Germany). NP were suspended in distilled water at a concentration of 10 mg/ml, dropped onto aluminum SEM stubs, and dried at room temperature. nCmP samples were placed on SEM stubs covered by double-sided adhesive carbon tabs. Samples were sputter coated with a thin film of gold/palladium alloy a BIO-RAD system at 20 μA for 60 seconds under argon gas. Images were captured at 5 kV at various magnifications.

### 2.7 Particle size, size distribution, and zeta potential analysis of NP and nCmP

The hydrodynamic size, size distribution (polydispersity index, PDI), and zeta potential of NP and NP re-dispersed from nCmP were measured by dynamic light scattering (DLS) using a Malvern Nano Zetasizer (Malvern Instruments, Worcestsershire, UK). NP were suspended in distilled water (0.5 mg/mL, pH 9), vortexed, and sonicated for one minute, and measurements were performed at 25°C. The sizes of dry NP and nCmP were analyzed by measuring the diameter of at least 100 particles from SEM images using ImageJ (Systat, San Jose, CA, USA).

### 2.8 Analysis of PTX loading in PTX NP and PTX nCmP

The drug loading (DL) of PTX NP and nCmP was determined via ultra-performance liquid chromatography (UPLC, LaChrom, Hitachi, Japan). The detection of PTX was performed using an Ascentis column ($C_{18}$, 5 μm × 150 mm × 4.6 mm). The UPLC conditions were as follows: pump rate of 1 ml/min, absorbance of 227 nm, temperature of 25°C, 20 μL per

injection, 4-minute retention time, and a mobile phase containing 60% acetonitrile and 40% DI water. Samples were completely dissolved in the mobile phase (1 mg/mL) prior to analysis. The PTX concentration was quantified by comparison with a standard calibration curve of PTX in the mobile phase. The drug loading, encapsulation efficacy (EE) and NP loadings were calculated using the following equations:

$$\mathrm{DL(wt\%)} = \frac{\text{mass of PTX in NP}}{\text{total mass of particles}} \times 100 \quad (1)$$

$$\mathrm{EE(wt\%)} = \frac{\text{actual drug loading}}{\text{theoretical drug loading}} \times 100 \quad (2)$$

$$\text{Theoretical drug loading(wt\%)} = \frac{\text{initial mass of PTX}}{\text{initial mass of PTX} + \text{initial mass of Ac} - \text{Dex}} \times 100 \quad (3)$$

$$\text{NP loading(wt\%)} = \frac{\text{mass of NP loaded in nCmP}}{\text{mass of nCmP}} \times 100 \quad (4)$$

$$\text{NP loading efficacy(wt\%)} = \frac{\text{mass of NP loaded in nCmP}}{\text{initial mass of NP in nCmP formulation}} \times 100 \quad (5)$$

### 2.9 *In vitro* PTX release from NP and nCmP

The *in vitro* release profiles of PTX from NP and nCmP were determined via a release study of suspended particles (1 mg/mL, 1.7 mL) in modified phosphate buffer (PBS, 0.1 M, pH 7.4, 0.5% wt% Tween 80) and modified acetate buffer (0.1 M, pH 5, 0.5% wt% Tween 80). The suspensions were incubated at 37°C and 100 rpm (Digital Heat Block and Orbi shaker, Benchmark Scientific, Edison, NJ, USA). At various time points (0–7 days), particle samples were centrifuged at 23,102 g for 5 minutes at 4°C to isolate the particles. 200 mL of supernatant was withdrawn and replaced by the same amount of fresh buffer. The supernatant samples were analyzed for PTX content by UPLC following the same method described previously.

### 2.10 Differential scanning calorimetry (DSC)

The thermal phase transitions of NP, nCmP, and raw materials were determined by DSC using a TA Q10 DSC system (TA instruments, New Castle, DE, USA) equipped with an automated computer-controlled cooling system. 1–3 mg of sample was weighed into Tzero™ alodine-coated aluminum pans, which were hermetically sealed. The sealed sample pan was placed in the DSC chamber along with an empty sealed reference pan, which were heated from 0–300 °C at a rate of 10 °C/min.

### 2.11 Powder X-ray diffraction (PXRD)

PXRD was applied to determine the crystalline nature of nCmP and its raw components using a Rigaku Multiflex X-ray diffractometer (The Woodlands, TX, USA) with Cu Kα radiation source (40KV, 44mA). Samples were placed in a horizontal slit holder prior to analysis. The scan range was 5–60° in 2θ at a sampling width of 0.1 and scan speed of 1°/min.

### 2.12 Karl Fischer coulometric titration

The water content of nCmP was quantified by Karl Fischer (KF) coulometric titration using a 737 KF coulometer (Metrohm, Riverview, FL, USA). 10 mg of particles were dissolved in anhydrous methanol and injected into the reaction cell filled with Hydranal® KF reagent. The water content was analyzed and reported in wt%. Pure solvent was analyzed as background sample.

### 2.13 *In vitro* aerosol dispersion performance with a Next Generation Impactor (NGI)

The *in vitro* aerosol dispersion of dry powder nCmP was evaluated using a Next Generation Impactor™ (NGI™, MSN Corporation, Shoreview, MN, USA) equipped with a stainless-steel induction port attachment (USP throat) and gravimetric NGI™ insert cups. The NGI was connected to a Copley HCP5 vacuum pump (Copley Scientific, United Kingdom). The flow rate was measured and adjusted to 60 L/min, which models the flow rate of healthy adult lungs.[38] Glass fiber filters (55 mm, type A/E, Pall Life Sciences) were weighed and placed on the insert cups from stages 1 through 7 to reduce bounce or re-placement of powder.[39] 10 mg of powder was loaded into a hydroxypropyl methylcellulose capsule (HPMC, size 3, Quali-V®, Qualicaps® Inc., Whitsett, NC, USA) and placed in a human dry powder inhaler (DPI) device (Handihaler, Boehringer Ingelheim Pharmacauticals, CT, USA). The DPI was then attached to a rubber mouthpiece connected to the NGI. Three capsules were released in every experiment (for a total of 30 mg) in triplicate. The NGI was operated with a delay time of 10 s and running time of 10 s. The particle deposition on each stage was determined gravimetrically by the difference in mass of the glass filter before and after particle deposition. The effective cutoff diameters for each impaction stage were given by the manufactured as: Stage 1 (8.06 μm); Stage 2 (4.46 μm); Stage 3 (2.82 μm); Stage 4 (1.66 μm); Stage 5 (0.94 μm); Stage 6 (0.55 μm); and Stage 7 (0.34 μm). The fine particle dose (FPD), fine particle fraction (FPF), respirable fraction (RF), and emitted dose (ED) were calculated as follows:

$$\text{Fine particle dose}(\text{FPD}) = \text{mass of particles} < 4.4\,\mu\text{m}\,(\text{stages 2 through 7}) \tag{6}$$

$$\text{Fine particle fraction}(\text{FPF}) = \frac{\text{fine particle dose}}{\text{initial particle mass loaded into capsules}} \times 100 \tag{7}$$

$$\text{Respirable fraction}(\text{RF}) = \frac{\text{mass of particles} < 4.4\,\mu\text{m (stages 2 through 7)}}{\text{total particle mass on all stages}} \times 100 \tag{8}$$

$$\text{Emitted dose (ED)} = \frac{\text{initial mass in capsules} - \text{final mass remaining in capsules}}{\text{initial mass in capsules}} \times 100 \quad (9)$$

The experimental mass median aerodynamic diameter ($MMAD_E$) and geometric standard deviation (GSD) for the particles were determined using a Mathematica® program written by Dr. Warren Finlay.[39]

### 2.14 Tapped density and theoretical aerodynamic size analysis of nCmP

The density of nCmP was determined via tapped density measurements.[40] 25–35 mg of particles (m) was weighed in a thin glass tube and tapped 200 times over a hard surface to ensure efficient packing. The height and diameter of compacted particles were measured using a digital caliper to calculate the volume occupied for the particles (V). The tapped density (r) was calculated using the equation:

$$\rho = \frac{m}{V} \quad (10)$$

The theoretical MMAD ($MMAD_T$) was calculated using the following equation:

$$MMAD_T = d\sqrt{\frac{\rho}{\rho^*}} \quad (11)$$

where d is the geometric diameter of nCmP determined by ImageJ and $\rho^* = 1\ g/cm^3$ is the reference density of solid polymer.

### 2.15 *In vitro* cell studies

A549 human epithelial adenocarcinoma lung cancer cells were cultured in DMEM containing 10 v/v % FBS, 1 mM sodium pyruvate, 1 v/v % penicillin streptomycin (100 U/ml penicillin, 100 μg/ml streptomycin), and 0.2 v/v % Fungizone (0.5 μg/ml amphotericin B, 0.41 μg/ml sodium deoxycholate). H441 cells were cultured in RPMI L-glutamine media containing same additives, except sodium pyruvate. Cells were incubated at saturated humidity, 37 °C, and 5% $CO_2$.

**2.15.1 Two-Dimensional (2D) cell culture and cell viability—**The viability of A549 cells exposed to free PTX and PTX NP was evaluated using a resazurin assay on 2D cell monolayers. Cells (5,000 cells/well) were seeded in a flat bottomed 96-well plate and allowed to attach for 24 hours. PTX was dissolved in DMSO and then serially diluted in media (final DMSO concentration < 0.2 v/v%). Cells were dosed with free PTX and PTX NP at concentrations from 0.001 – 10 μM PTX for 48 hours. Resazurin was added to the wells (20 μL, 20 mM) and incubated for 4 hours. The fluorescence intensity was detected at 544/590 nm in a Cytation 3 plate reader (BioTek Instruments Inc., Winooski, VT, USA). Relative viability was expressed as the fluorescence of cells dosed with PTX formulations over control cells.

**2.15.2 NP cellular uptake—**Confocal microscopy images were taken of A549 cells seeded on 35 mm glass bottom Petri dishes at a concentration of 500,000 cells/dish incubated overnight. Cells were exposed to 66 μM CUR NP and incubated for 3 hours, washed 3X with PBS, stained with CellMask™ deep red plasma membrane (0.5 μL/mL in PBS), and fixed with 4% paraformaldehyde in PBS. Images were taken at 100X magnification. For quantification, A549 cells were seeded in flat bottomed 96-well plate (5,000 cell/well), incubated for 24 hours, and dosed with 66 μM CUR NP. After 3 hours of incubation, cells were washed twice with 200 mM glycine in PBS, twice with cold PBS, and fixed with 200-proof ethanol for 10 minutes. NP uptake was quantified using a fluorescence scan at 420/540 nm.

**2.15.3 Transepithelial electrical resistance (TEER) evaluation—**Transepithelial electrical resistance was applied on the alveolar epithelium cell line H441[41] to evaluate monolayer integrity following nCmP exposure. 100,000 cells/well were seeded on the apical side of a 0.4 μm Transwell and grown in liquid covered culture for two days. Air interface culture was induced when media was removed from the apical side of the Transwells. TEER values were measured periodically until a tight monolayer was formed (stable TEER values), and Blank and PTX nCmP (1 mg/well) were dosed to the cells (day 0). TEER readings continued for five days and treated samples were compared to control cells.

**2.15.4 Liquid covered culture 3D multicellular spheroid (MCS) evaluation—**3D multicellular spheroids (MCS) were formed via centrifugation using A549 cells for the evaluation of PTX NP. 5,000 cells/well containing collagen type I (20 μL/mL cell solution) were seeded into ultra-low attachment round-bottomed 96-well plates, centrifuged at 1100 g for 15 minutes, and incubated. At day 5, fully-formed MCS were dosed with free PTX and PTX NP (5 – 0.001 μM PTX), Blank NP, 0.1% DMSO in media, and media (control). Bright-field images were taken using a Cytation 3 imager (BioTek Instruments Inc., Winooski, VT, USA) at different time points over 15 days, and the diameter of MCS were evaluated. The growth or inhibition of MCS upon PTX exposure was analyzed by calculating the change in size in treated MCS relative to untreated controls.

**2.15.5 Air interface culture 3D multicellular spheroid (MCS) evaluation—**For the evaluation of aerosolized PTX nCmP, A549 cells were seeded into an alginate scaffold and grown in air interface culture (AIC) conditions. Alginate was purified as previously described.[42] 3 mL of 1.65 wt% alginate in PBS was loaded into a 5 mL syringe, and all bubbles were removed. In another 5 mL syringe, 750 μL of 150 mM $CaSO_4$ in PBS containing 1% (v/v) Fungizone was collected. The syringes were connected and vigorously mixed. The resulting mixture was transferred into 3D Petri Dishes® (5 × 7 array, 800 × 800 μm, MicroTissue, Providence, RI, USA) to form hydrogel micromolds. Excess solution was removed from the top of the mold and gelation occurred at room temperature for 15–20 minutes. Once the alginate scaffold gelled, it was removed from the mold and incubated overnight in DMEM prior to seeding. The Young's modulus of the alginate gels was determined using an Instron 3342 single-column apparatus (Norwood, MA) with a strain rate of 2 mm/min until hydrogel failure. The Young's modulus was calculated from the slope

of the linear region of the resulting stress-strain curve using Instron's Bluehill 3 software package.

Alginate scaffold micromolds were placed in Transwell® inserts (3.0 μm pore size, 12-well plates). 500 μL of DMEM was transferred to the basolateral compartment of the Transwell, and 75 μL of cell solution ($1.33 \times 10^6$ cell/ml) was transferred to the hydrogel scaffold (apical side). After MCS formation (day 1), media in the scaffold was gently removed to allow the MCS to grow in AIC conditions. Media from the basolateral side was replaced every other day. At day 5, PTX nCmP, equivalent to 1 μM and 5 μM of PTX in mass, were dosed onto the AIC MCS in powder form using a syringe and cone for dispersion, as can be seen in Figure 1. Blank nCmP with equivalent mass to PTX nCmP doses were also dispersed onto AIC MCS. Images were taken periodically using the Cytation3 imager from days 1 to 15. The diameter of MCS treated with PTX nCmP was recorded and compared to untreated controls. The growth or inhibition of AIC MCS upon nCmP exposure was analyzed by calculating the change in size in treated MCS relative to untreated control.

### 2.16 Statistical analysis

All measurements were performed in at least triplicate and values were presented as mean ± standard deviation. Half maximal inhibitory concentration ($IC_{50}$) values were calculated using a symmetrical sigmoidal fit method in readerfit.com. The statistical significance of the results was determined using Student's t-test, where $p < 0.05$ (*) was considered statistically significant.

## 3. RESULTS

### 3.1 Characterization of acetalated dextran (Ac-Dex)

The synthesis of Ac-Dex resulted from the reaction between dextran and 2-MOP in the presence of an acid catalyst, and the resulting hydrophobic polymer contained both cyclic and acyclic acetal groups. NMR analysis showed a total acetal coverage (conversion of -OH groups) of 81% and a cyclic acetal coverage of 80.5 (per 100 glucose units). Figure S1 and Table S1 show a representative spectrum and the detailed results of $^{+}$H NMR, respectively.

### 3.2 Nanoparticle characterization

**3.2.1 Morphology, size, size distribution, and surface charge—**The size, distribution, and surface charge of NP are presented in Table 1. For PTX NP and Blank NP, the hydrodynamic diameters were less than 200 nm with low PDI (< 0.15) and slightly negative charges. PTX NP were spherical and smooth with uniform dispersion as shown in Figure 2A. ImageJ size analysis from the SEM micrographs indicated smaller NP sizes for both PTX NP and Blank NP.

**3.2.2 PTX loading and *in vitro* release—**PTX was encapsulated into Ac-Dex NP with an encapsulation efficiency of 71% and drug loading of 3.57 wt% (Table 1). The release profile of PTX NP (Figure 2D) demonstrated sustained release of PTX, with a slight burst release for both pH values. PTX release was slower at pH 7.4, reaching 47% release in

7 days. In contrast, release at pH 5.1 was faster, reaching a plateau at 48 hours with around 70% PTX release.

## 3.3 Nanocomposite microparticle characterization

**3.3.1 Morphology, size, surface charge, and re-dispersion—**PTX nCmP exhibited raisin-like morphology (Figure 2B) with visible nanoparticles (Figure 2C). The geometric diameter of nCmP determined using ImageJ was 2.17 μm (Table 2). PTX NP re-dispersed from PTX nCmP exhibited an increase in size to 270.6 nm, higher PDI of 0.33, and a more negative charge (−18.5 mV) (Table 1).

**3.3.2 Drug loading, loading efficacy, and *in vitro* release from nCmP—**PTX nCmP had a drug loading of 3.04 wt%, corresponding to a PTX loading efficacy of 105 % in nCmP (Table 2). PTX nCmP exhibited sustained release of PTX at both pH values, with accelerated release in acidic conditions similar to PTX NP (Figure 2D).

**3.3.3 Water content analysis—**The residual water content of PTX nCmP was lower than 3% (Table 2), determined via colorimetric Karl Fischer titration.

**3.3.4 Solid-state analysis of particle formulations—**DSC thermograms of raw materials and nCmP are shown in Figure 3A. Raw PTX exhibited an endothermic phase transition peak at 222 °C and an exothermic peak at 243 °C. Raw Ac-Dex presented a broad endothermic peak around 183°C and raw mannitol displayed a main phase transition peak at 171°C. Blank and PTX nCmP showed similar broad peaks around 158 and 188 °C and no phase transitions were observed for any samples under 150 °C. Figure 3B presents powder X-ray diffractograms of raw materials and nCmP. Raw Ac-Dex presented no peaks, and raw PTX and mannitol exhibited strong peaks. After spray drying, blank and PTX nCmP exhibited no significant peaks.

**3.3.5 Density and theoretical MMAD of nCmP—**The tapped density and the theoretical mass median aerodynamic diameter ($MMAD_T$) of PTX nCmP are shown in Table 2. The corresponding values were 0.33 g/cm$^3$ and 1.25 ± 0.01 μm.

**3.3.6 *In vitro* aerosol performance of nCmP—**The *in vitro* aerosol dispersion analysis of PTX nCmP showed broad aerosol dispersion of particles across all stages (Figure 4A), with 3% of the total mass depositing on the first stage, the majority of nCmP deposited on stage 4 (35%), and 4% depositing on at stage 7. The experimental MMAD was 2.44 μm, with a GSD of 2.34 μm (Table 2). The FPF, RF and ED were 66, 97, and 88%, respectively (Figure 4B).

## 3.4 *In vitro* cell analysis of PTX NP and PTX nCmP

**3.4.1 *In vitro* cytotoxicity in 2D monolayer—**A 2D monolayer of A549 cells exposed to free PTX and PTX NP exhibited $IC_{50}$ values of 0.23 μM and 0.07 μM PTX NP, respectively, after 48 hours of exposure (Figure 5A).

**3.4.2 Cellular uptake of CUR NP—**The cellular uptake of NP into 2D A549 cells was evaluated using fluorescent CUR NP with similar size, PDI, and surface charge to PTX NP. Figure 5B shows a representative confocal image of CUR NP associated in the cytoplasm of A549 cells, and the quantification of CUR NP uptake indicated that more CUR NP were successfully uptaken into A549 cells.

**3.4.3 Transepithelial electrical resistance (TEER) evaluation—**The effect of PTX and Blank nCmP on cell monolayer integrity in air interface culture (AIC) conditions was evaluated via transepithelial electrical resistance (TEER). The AIC monolayer reached TEER values above 100 Ω $cm^2$ a day after transitioning from LCC to AIC conditions, and these values remained stable until analysis began (Figure 5C). For the first two days after exposure to nCmP, cells exposed to Blank nCmP exhibited increased relative TEER, which then decreased slightly and was statistically the same as the control TEER. Cells exposed to PTX nCmP showed no statistical difference in TEER during the 5-day evaluation in comparison to the control.

**3.4.4 Liquid covered culture (LCC) MCS growth inhibition evaluation—**LCC 3D A549 multicellular spheroids (MCS) dosed with free PTX and PTX NP exhibited a dose dependent response in the inhibition of the growth of MCS in comparison to the control (Figure 6). In particular, MCS experienced growth inhibition when exposed to PTX concentrations equal to or above 0.01 μM for both free PTX and PTX NP. Figure 6C shows the comparison in the change of MCS diameter with respect to the control. Between 0.01 and 0.5 μM PTX the MCS had similar responses to free PTX and PTX NP, where MCS size decreased with increasing PTX concentration by day 15. At higher PTX concentrations (≥ 1 μM), MCS exposed to free PTX reached a plateau where MCS size no longer decreased, and MCS exposed to PTX NP continued to decrease in size. Figure 7 shows representative images of LCC MCS dosed with 1 μM PTX at different time points, and their corresponding sizes. The MCS were not tightly formed on day 1 and increased in size and solidarity with time. For days 1 and 5, the size of the MCS exposed to free PTX and PTX NP were similar to the control, whereas by day 15, MCS size decreased significantly upon exposed to free PTX and PTX NP. The effect of Blank NP on MCS growth was also evaluated, showing no significant difference to control MCS, with the exception of being slightly larger than the control MCS after 15 days (Figure 7B).

**3.4.5 AIC MCS growth inhibition evaluation—**As shown in Figure 1, air interface culture (AIC) MCS were formed on alginate micromolds prior to exposure to aerosolized nCmP. The alginate micromold scaffolds exhibited a Young's modulus of 3.55 ± 0.59 kPa after 24 hours of incubation in DMEM. A549 cells seeded in the alginate micromold were transitioned to AIC a day after seeding in LCC. At day 5, the spheroids were compact and fully formed (Figure 8A), and thus AIC MCS were exposed to nCmP at this time. After dosing with nCmP the MCS showed gradual tumor size reduction and disaggregation at the highest PTX nCmP concentration (5 μM) in comparison to control MCS. The change in diameter of AIC MCS from day 5 to day 15 are reported in Figure 8B (MCS diameters from day 3 to 15 can be found in Figure S1). MCS exposed to Blank nCmP exhibited a high growth rate than the control, whereas PTX nCmP resulted in no growth in the AIC MCS.

The change in diameter of AIC MCS relative to control after the treatment on day 15 can be seen in Figure 8C. Blank nCmP did not show any significant effect on the growth of AIC MCS, and both PTX nCmP formulations resulted in effectively no growth in the MCS at this time point.

## 4. DISCUSSION

Water-soluble dextran was transformed to hydrophobic Ac-Dex, where parent -OH groups were converted into acetal groups. Ac-Dex had a high total -OH conversion that can help to ensure the stability of particles and allow for the formation of small NP.[40] The resulting acetal groups allows the NP to have pH-tunable degradation for drug delivery in acidic tumors or inflammatory tissues.[43]

The small size of PTX NP reported from the SEM and ImageJ represent NP in their dry state. The hydrodynamic size of PTX NP evaluated with DLS allowed for the measurement of NP size with a hydrated layer. PTX NP had a low PDI, indicating high NP stability in an aqueous suspension due to the steric effect of the PVA coating.[44] SEM images of NP corroborates the high homogeneity reached with single emulsion fabrication. After spray drying, NP re-dispersed from nCmP showed a 35% increase in hydrodynamic diameter, likely due to agglomeration during the spray drying process, which is confirmed by a higher PDI. The slightly more negative charge of re-dispersed PTX NP can be attributed to mannitol in the formulation, which showed a charge of around −19.23 mV in water solution, compared to the almost neutrally-charged PTX NP.

The *in vitro* PTX release profiles of the NP and nCmP were evaluated in physiological (pH 7.4) and acidic (pH 5.1) conditions. The systems exhibited a low initial burst release, which is an essential characteristic for extended-release delivery systems.[45] The release profiles at each pH were similar between the NP and nCmP. In acidic conditions, the majority of PTX was released after 48 hours. At pH 7.4, PTX release was slower, reaching 50% release after 7 days. Fast PTX release in lower pH and slower release in neutral pH can be favorable for fast release of the drug in the acidic microenvironments of cancer cells while having slower release in healthy tissue.

PTX NP exhibited high PTX encapsulation efficiency, and after spray drying the PTX loading in nCmP increased, which corresponds to a NP loading efficiency in nCmP above 100%. This phenomenon is likely due to the loss of PVA from the NP during the spray drying process, which leads to an increase in the percentage of PTX in the total nCmP mass. The low water content in PTX nCmP can enable storage stability of the particles, and can prevent agglomeration during aerosolization.

DSC analysis was performed for raw materials and nCmP to evaluate their stability and phase transition behavior. The lack of an endothermic peak at 222°C and decomposition peak at 243°C (evident for raw PTX) in PTX nCmP suggests that amorphization of the drug occurred during spray drying or that the amount of PTX in the nCmP was below the detection limit for DSC. The strong endothermic peak from pure mannitol was not present for the nCmP. The broad peak present for nCmP is likely due to displacement of the Ac-Dex

phase transition peak. Overall, nCmP showed temperature stability under 150°C to comply with manufacturing and storage conditions.

The crystallinity of raw materials and nCmP were analyzed by PXRD. The lack of peaks in the Ac-Dex diffractogram indicate that it is an amorphous polymer, which is likely because of the rapid precipitation method of collection after the Ac-Dex reaction. While raw PTX and mannitol exhibited strong peaks and are thus crystalline, these peaks are no longer present in nCmP. This indicates the likelihood of amorphization of PTX and mannitol after the spray drying process. These data agree with the reduced and transformed peaks observed in DSC analysis. Reduced crystallinity of the nCmP formulation is advantageous for the rapid solubilization of nCmP formulations (and thus release of PTX) after delivery to the lungs.

The *in vitro* aerosol performance of PTX nCmP was conducted using a Next Generation Impactor™ coupled with a human DPI device. The simulated inhalation resulted in a high emitted dose of particles, which is necessary to make use of the most of each dosage. The fine particle fraction of PTX nCmP indicates that 66% of the nCmP mass released from the capsules had a particle size lower than 4.4 μm, and the 97% RF demonstrates the potential for effective deposition of particles to the bronchi and distal airways. nCmP that deposited on the first stage of the NGI (3%) would likely deposit primarily by impaction (≥ 5 μm) in the upper respiratory airways (primary bronchi) of the lungs.[12] Particles that deposited in stages 2 to 6, corresponding to 93% to the total mass in all stages of the NGI, would likely be able to deposit in the lower lung airways (secondary bronchi and bronchioles) due to sedimentation (0.5 – 5 μm), and the smaller particles from stage 7 would likely deposit via Brownian motion in the alveoli region (< 0.5 μm).[11] The high dispersion of nCmP (GSD of 2.34 μm) demonstrates the ability of nCmP to deposit in all stages of the NGI.

The theoretical mass median aerodynamic diameter ($MMAD_E$ of 1.25 μm) was calculated from the geometric diameter from SEM micrographs and tapped density of the PTX nCmP, and was smaller than the experimental MMAD obtained using the NGI, with an increase of 95%. The increase in MMAD following aerosolization in the NGI is likely due to agglomeration of the particles due to ambient humidity and the electrostatic interactions of amongst the particles,[46] which can increase particle deposition in the upper airways.[47] The deposition of the PTX nCmP in lower stages was likely achieved because of their low tapped density, which can be attributed to the raisin-like morphology of the nCmP. The hollow shell morphology of the nCmP can be attributed to the saturation of NP at the droplet surface compared to the droplet center, where NP diffusion is slower than the surface shrinkage during spray drying. As the evaporation process occurs, the droplet shell collapses and wrinkled particles with low density are formed,[48] as observed in the PTX nCmP.

The cytotoxicity of free PTX and PTX NP was evaluated in LCC monolayers. 2D A549 cells were dosed with free PTX and PTX NP and there was a 70% reduction in the $IC_{50}$ value for PTX NP compared to free PTX after 48 hours of exposure, suggesting that the sustained release of the drug plays a role in enhancing cell death.[45]

For cellular uptake, CUR NP were selected for their similar size and charge to PTX NP and the ease in imaging fluorescent CUR without negatively impacting cell viability and morphology. Since NP surface charge is nearly neutral, the main parameter that can influence NP internalization in cells is their size. It was previously reported that 100–200 nm polymeric NP might be the optimal size for the highest uptake in cells and to avoid alveolar macrophage clearance.[49] CUR NP were successfully uptaken into the A549 cytoplasm after three hours of exposure, indicating the NP have the potential to deliver and release PTX directly inside the cells.

In order to determine the effects of Blank and PTX nCmP on the lung epithelium, we evaluated the integrity of the tight junctions of an air interface monolayer of H441 cells upon exposure to nCmP via transepithelial electrical resistance (TEER) measurements. H441 cells were grown in a monolayer as a human distal lung epithelial model,[50] and following growth in AIC, were dosed with nCmP powders. The increase in TEER upon exposure to Blank nCmP is likely due to exposure of the cells to the by-product dextran following the degradation of Ac-Dex as nutrient for the cells. Cells exposed to PTX nCmP did not show significant reduction in TEER for up to 5 days of exposure, suggesting a conservation in the tight junctions in the monolayer of cells.

While 2D cell culture has been extensively used for drug screening, a 3D multicellular spheroid (MCS) platform offers a better representation of solid tumors *in vitro* due to their similar structures, physiological responses, cell-drug interactions, and drug resistance mechanisms.[51–52] MCS grown in a 3D LCC model were dosed with free PTX and PTX NP 5 days after MCS formation. MCS at this point were fully developed spheroids with heterogenous structure: a proliferating region, a quiescent viable region, and a necrotic core. This phenomenon has been confirmed in our previous work and is in accordance with other reports where MCS > 200 μm have shown similar characteristics to real tumors.[30, 32] MCS growth continued for 15 days, as after this point control MCS size begins to decline.

PTX NP showed no clear superiority in the inhibition of MCS growth in comparison to free PTX, implying that PTX NP are as effective as free PTX, with both likely experiencing limited penetration into the MCS. The likelihood of limited penetration in the MCS is supported by the fact that tumors develop a dense extracellular matrix (ECM) that prevents the transport and diffusion of large molecules into their interstitial space.[53–54] Collagen, one of the main components in ECM, is known to increase the resistance to interstitial transport in tumors.[55] The described LCC MCS contained type I collagen to facilitate the agglomeration of cells. The formation of a solid external cell layer in the spheroids was visible in the bright-field images when they changed from loose aggregates of cells to solid tumor spheroids from day 1 to day 5. In addition, MCS exposure to Blank NP did not result in alterations in the growth of the MCS, likely due to their exposure to the harmless by-products of Ac-Dex degradation, which can cause an increase in MCS size as they can use dextran as a nutrient.

To demonstrate proof-of-concept treatment of lung cancer via aerosol delivery of PTX-loaded dry powders, PTX NP were spray dried with mannitol to obtain nCmP, which can be delivered using a dry powder inhaler. To evaluate the chemotherapeutic effect of the

particles, MCS grown in an alginate micromold scaffold at air interface culture (AIC) conditions were dosed with dry powder PTX nCmP. The alginate scaffold exhibited similar stiffness to that of lung tissue, which has a Young's modulus between 1 and 5 kPa.[56] Immediately after PTX nCmP treatment (day 5) and up to day 15 the MCS sizes were significantly inhibited with no appreciable growth. MCS exposed to PTX nCmP displayed disaggregation of cells as signal of cell death promoted by PTX delivered from the NP. Blank nCmP seemed to increase MCS growth in comparison to the control.

Although the overall cytotoxicity of PTX NP and PTX nCmP was found to be comparable to that of free PTX, the encapsulation of the drug into the nanocarrier and further nCmP formulation is key for the development of a stable dry powder formulation with appropriate lung deposition, reduced physiological clearance and effective tumor inhibition for a localized delivery of the drug. Overall, this formulation show promise in the treatment of lung cancer via a pulmonary route. PTX nCmP have the potential to reduce the total dose administered and reach the targeted site of the disease in comparison to systemic delivery.

## 5. CONCLUSIONS

We developed a paclitaxel-loaded aerosol nanocomposite microparticle (PTX nCmP) formulation based on spray-dried Ac-Dex PTX-loaded NP and mannitol. PTX nCmP exhibited favorable *in vitro* aerosol distribution and deposition using an NGI, with a size and morphology that can allow them to reach the distal regions of the lungs. NP were successfully re-dispersed from nCmP upon contact with aqueous medium. The physical properties of the NP allowed for effective cellular uptake in A549 cells. 2D cells were highly affected by PTX NP is comparison to free PTX, however, this correlation was not seen in the 3D LCC model. This phenomenon demonstrates the complex interaction of nanoparticles with MCS. The 3D AIC platform allowed for the assessment of PTX nCmP, showing its potential as an *in vitro* model to better mimic pulmonary environments and promoting its further application in the evaluation of other aerosol formulations. Overall, the described work involves a new nCmP platform capable of effectively delivering PTX to the lungs via their aerosolization as a dry powder.

## Supplementary Material

Refer to Web version on PubMed Central for supplementary material.

## ACKNOWLEDGEMENTS

The authors thank RIN$^2$ for SEM and XRD access. Research reported in this publication was partially supported by the Institutional Development Award (IDeA) Network for Biomedical Research Excellence from the National Institute of General Medical Sciences of the National Institutes of Health under grant number P20GM103430. In addition, this work was made possible by the use of equipment and services available through the RI-INBRE Centralized Research Core Facility. This material is based upon work conducted at a Rhode Island NSF EPSCoR research facility, supported in part by the National Science Foundation EPSCoR Cooperative Agreement #EPS-1004057. This material is also based in part upon work supported by the National Science Foundation under grant #1508868. Any opinions, findings, and conclusions or recommendations expressed in this material are those of the authors and do not necessarily reflect the view of the National Science Foundation or National Institutes of Health.

## ABBREVIATIONS

| | |
|---|---|
| **PTX** | paclitaxel; NP, nanoparticles |
| **Ac-Dex** | acetalated dextran |
| **CUR** | curcumin |
| **CAC** | cyclic acetal coverage |
| **2D** | two-dimensional |
| **3D** | three-dimensional |
| **MCS** | multicellular tumor spheroids |
| **PPTS** | pyridinium p-toluenesulfonate |
| **DMSO** | dimethyl sulfoxide |
| **2-MOP** | 2-methoxypropene |
| **TEA** | triethylamine |
| **DCM** | dichloromethane |
| **PVA** | poly(vinyl alcohol) |
| **PBS** | phosphate buffered saline (1X PBS dilution unless specified) |
| **NMR** | nuclear magnetic resonance |
| **DLS** | dynamic light scattering |
| **PDI** | polydispersity index |
| **DL** | drug loading |
| **EE** | encapsulation efficacy |
| **UPLC** | ultra-performance liquid chromatography |
| **DMEM** | Dulbecco’s modified Eagle’s medium |
| **RPMI** | Roswell Park Memorial Institute |
| **FBS** | fetal bovine serum |
| **DSC** | differential scanning calorimetry |
| **PXRD** | powder X-ray diffraction |
| **KF** | Karl Fischer titration |
| **NGI** | Next Generation Impactor |
| **FPD** | fine particle dose |

| | |
|---|---|
| **FPF** | fine particle fraction |
| **RF** | respirable fraction |
| **ED** | emitted dose |
| **DPI** | dry powder inhaler |
| **LCC** | liquid covered culture |
| **AIC** | air interface culture |

## REFERENCES


1. Siegel RL; Miller KD; Jemal A, Cancer statistics, 2019. CA Cancer J Clin 2019, 69 (1), 7–34. DOI: 10.3322/caac.21551. [PubMed: 30620402]
2. Mansour HM; Rhee YS; Wu X, Nanomedicine in pulmonary delivery. International journal of nanomedicine 2009, 4, 299–319. [PubMed: 20054434]
3. Patil JS; Sarasija S, Pulmonary drug delivery strategies: A concise, systematic review. Lung India 2012, 29 (1), 44–9. DOI: 10.4103/0970-2113.92361. [PubMed: 22345913]
4. Labiris NR; Dolovich MB, Pulmonary drug delivery. Part I: physiological factors affecting therapeutic effectiveness of aerosolized medications. Br J Clin Pharmacol 2003, 56 (6), 588–99. [PubMed: 14616418]
5. Ali M, CHAPTER 9 - Pulmonary Drug Delivery In Handbook of Non-Invasive Drug Delivery Systems, Kulkarni VS, Ed. William Andrew Publishing: Boston, 2010; pp 209–246. DOI: 10.1016/B978-0-8155-2025-2.10009-5.
6. Abdelaziz HM; Gaber M; Abd-Elwakil MM; Mabrouk MT; Elgohary MM; Kamel NM; Kabary DM; Freag MS; Samaha MW; Mortada SM; Elkhodairy KA; Fang JY; Elzoghby AO, Inhalable particulate drug delivery systems for lung cancer therapy: Nanoparticles, microparticles, nanocomposites and nanoaggregates. J Control Release 2018, 269, 374–392. DOI: 10.1016/j.jconrel.2017.11.036. [PubMed: 29180168]
7. Hadinoto K; Phanapavudhikul P; Kewu Z; Tan RBH, Dry powder aerosol delivery of large hollow nanoparticulate aggregates as prospective carriers of nanoparticulate drugs: Effects of phospholipids. International Journal of Pharmaceutics 2007, 333 (1–2), 187–198. DOI: 10.1016/j.ijpharm.2006.10.009. [PubMed: 17084567]
8. van Rijt SH; Bein T; Meiners S, Medical nanoparticles for next generation drug delivery to the lungs. European Respiratory Journal 2014, 44 (3), 765 DOI: 10.1183/09031936.00212813. [PubMed: 24791828]
9. Fernández Tena A; Casan Clarà P, Deposition of Inhaled Particles in the Lungs. Archivos de Bronconeumología (English Edition) 2012, 48 (7), 240–246. DOI: 10.1016/j.arbr.2012.02.006.
10. Laube BL; Janssens HM; de Jongh FHC; Devadason SG; Dhand R; Diot P; Everard ML; Horvath I; Navalesi P; Voshaar T; Chrystyn H, What the pulmonary specialist should know about the new inhalation therapies. European Respiratory Journal 2011, 37 (6), 1308 DOI: 10.1183/09031936.00166410. [PubMed: 21310878]
11. Ngan CL; Asmawi AA, Lipid-based pulmonary delivery system: a review and future considerations of formulation strategies and limitations. Drug Deliv Transl Res 2018, 8 (5), 1527–1544. DOI: 10.1007/s13346-018-0550-4. [PubMed: 29881970]
12. Yang W; Peters JI; Williams RO, Inhaled nanoparticles—A current review. International Journal of Pharmaceutics 2008, 356 (1), 239–247. DOI: 10.1016/j.ijpharm.2008.02.011. [PubMed: 18358652]
13. Paranjpe M; Muller-Goymann CC, Nanoparticle-mediated pulmonary drug delivery: a review. Int J Mol Sci 2014, 15 (4), 5852–73. DOI: 10.3390/ijms15045852. [PubMed: 24717409]

14. Zhang J; Wu L; Chan H-K; Watanabe W, Formation, characterization, and fate of inhaled drug nanoparticles. Advanced Drug Delivery Reviews 2011, 63 (6), 441–455. DOI: 10.1016/j.addr.2010.11.002. [PubMed: 21118707]
15. Ungaro F; d'Angelo I; Coletta C; d'Emmanuele di Villa Bianca R; Sorrentino R; Perfetto B; Tufano MA; Miro A; La Rotonda MI; Quaglia F, Dry powders based on PLGA nanoparticles for pulmonary delivery of antibiotics: Modulation of encapsulation efficiency, release rate and lung deposition pattern by hydrophilic polymers. Journal of Controlled Release 2012, 157 (1), 149–159. DOI: 10.1016/j.jconrel.2011.08.010. [PubMed: 21864595]
16. Kunda NK; Alfagih IM; Miyaji EN; Figueiredo DB; Goncalves VM; Ferreira DM; Dennison SR; Somavarapu S; Hutcheon GA; Saleem IY, Pulmonary Dry Powder Vaccine of Pneumococcal Antigen Loaded Nanoparticles. Int J Pharm 2015 DOI: 10.1016/j.ijpharm.2015.09.034.
17. Restani RB; Pires RF; Tolmatcheva A; Cabral R; Baptista PV; Fernandes AR; Casimiro T; Bonifácio VDB; Aguiar-Ricardo A, POxylated Dendrimer-Based Nano-in-Micro Dry Powder Formulations for Inhalation Chemotherapy. ChemistryOpen 2018, 7 (10), 772–779. DOI: 10.1002/open.201800093. [PubMed: 30338202]
18. Restani RB; Silva AS; Pires RF; Cabral R; Correia IJ; Casimiro T; Bonifácio VDB; Aguiar-Ricardo A, Nano-in-Micro POxylated Polyurea Dendrimers and Chitosan Dry Powder Formulations for Pulmonary Delivery. Particle & Particle Systems Characterization 2016, 33 (11), 851–858. DOI: 10.1002/ppsc.201600123.
19. Wang Z; Meenach SA, Optimization of Acetalated Dextran-Based Nanocomposite Microparticles for Deep Lung Delivery of Therapeutics via Spray-Drying. J Pharm Sci 2017, 106 (12), 3539–3547. DOI: 10.1016/j.xphs.2017.07.022. [PubMed: 28827039]
20. Jiménez-López J; El-Hammadi MM; Ortiz R; Cayero-Otero MD; Cabeza L; Perazzoli G; Martin-Banderas L; Baeyens JM; Prados J; Melguizo C, A novel nanoformulation of PLGA with high non-ionic surfactant content improves in vitro and in vivo PTX activity against lung cancer. Pharmacological Research 2019, 141, 451–465. DOI: 10.1016/j.phrs.2019.01.013. [PubMed: 30634051]
21. Sofias AM; Dunne M; Storm G; Allen C, The battle of "nano" paclitaxel. Advanced Drug Delivery Reviews 2017, 122, 20–30. DOI: 10.1016/j.addr.2017.02.003. [PubMed: 28257998]
22. Xu X; Farach-Carson MC; Jia X, Three-dimensional in vitro tumor models for cancer research and drug evaluation. Biotechnol Adv 2014, 32 (7), 1256–68. DOI: 10.1016/j.biotechadv.2014.07.009. [PubMed: 25116894]
23. Senthebane DA; Jonker T; Rowe A; Thomford NE; Munro D; Dandara C; Wonkam A; Govender D; Calder B; Soares NC; Blackburn JM; Parker MI; Dzobo K, The Role of Tumor Microenvironment in Chemoresistance: 3D Extracellular Matrices as Accomplices. International journal of molecular sciences 2018, 19 (10), 2861 DOI: 10.3390/ijms19102861.
24. Septiadi D; Crippa F; Moore TL; Rothen-Rutishauser B; Petri-Fink A, Nanoparticle–Cell Interaction: A Cell Mechanics Perspective. Advanced Materials 2018, 30 (19), 1704463 DOI: 10.1002/adma.201704463.
25. Varan G; Patrulea V; Borchard G; Bilensoy E, Cellular Interaction and Tumoral Penetration Properties of Cyclodextrin Nanoparticles on 3D Breast Tumor Model. Nanomaterials (Basel, Switzerland) 2018, 8 (2), 67 DOI: 10.3390/nano8020067.
26. Minchinton AI; Tannock IF, Drug penetration in solid tumours. Nat Rev Cancer 2006, 6 (8), 583–92. DOI: 10.1038/nrc1893. [PubMed: 16862189]
27. Sant S; Johnston PA, The production of 3D tumor spheroids for cancer drug discovery. *Drug Discovery Today*: Technologies 2017, 23, 27–36. DOI: 10.1016/j.ddtec.2017.03.002. [PubMed: 28647083]
28. Katt ME; Placone AL; Wong AD; Xu ZS; Searson PC, In Vitro Tumor Models: Advantages, Disadvantages, Variables, and Selecting the Right Platform. Frontiers in bioengineering and biotechnology 2016, 4, 12–12. DOI: 10.3389/fbioe.2016.00012. [PubMed: 26904541]
29. Goodman TT; Ng CP; Pun SH, 3-D tissue culture systems for the evaluation and optimization of nanoparticle-based drug carriers. Bioconjugate chemistry 2008, 19 (10), 1951–1959. DOI: 10.1021/bc800233a. [PubMed: 18788773]

30. Nath S; Devi GR, Three-dimensional culture systems in cancer research: Focus on tumor spheroid model. Pharmacol Ther 2016, 163, 94–108. DOI: 10.1016/j.pharmthera.2016.03.013. [PubMed: 27063403]
31. Hamilton G, Multicellular spheroids as an in vitro tumor model. Cancer Letters 131 (1), 29–34. DOI: 10.1016/S0304-3835(98)00198-0.
32. Mehta G; Hsiao AY; Ingram M; Luker GD; Takayama S, Opportunities and Challenges for use of Tumor Spheroids as Models to Test Drug Delivery and Efficacy. J Control Release 2012, 164 (2), 192–204. DOI: 10.1016/j.jconrel.2012.04.045. [PubMed: 22613880]
33. Knight E; Przyborski S, Advances in 3D cell culture technologies enabling tissue-like structures to be created in vitro. Journal of Anatomy 2015, 227 (6), 746–756. DOI: 10.1111/joa.12257. [PubMed: 25411113]
34. Zanoni M; Piccinini F; Arienti C; Zamagni A; Santi S; Polico R; Bevilacqua A; Tesei A, 3D tumor spheroid models for in vitro therapeutic screening: a systematic approach to enhance the biological relevance of data obtained. Scientific Reports 2016, 6, 19103 DOI: 10.1038/srep1910310.1038/srep19103https://www.nature.com/articles/srep19103#supplementary-informationhttps://www.nature.com/articles/srep19103#supplementary-information . [PubMed: 26752500]
35. Costa EC; Moreira AF; de Melo-Diogo D; Gaspar VM; Carvalho MP; Correia IJ, 3D tumor spheroids: an overview on the tools and techniques used for their analysis. Biotechnology Advances 2016, 34 (8), 1427–1441. DOI: 10.1016/j.biotechadv.2016.11.002. [PubMed: 27845258]
36. Broaders KE; Cohen JA; Beaudette TT; Bachelder EM; Frechet JMJ, Acetalated dextran is a chemically and biologically tunable material for particulate immunotherapy. Proceedings of the National Academy of Sciences of the United States of America 2009, 106 (14), 5497–5502. DOI: 10.1073/pnas.0901592106. [PubMed: 19321415]
37. Wang Z; Meenach SA, Synthesis and Characterization of Nanocomposite Microparticles (nCmP) for the Treatment of Cystic Fibrosis-Related Infections. Pharm Res 2016, 33 (8), 1862–72. DOI: 10.1007/s11095-016-1921-5. [PubMed: 27091030]
38. Mahler DA, Peak Inspiratory Flow Rate as a Criterion for Dry Powder Inhaler Use in Chronic Obstructive Pulmonary Disease. Annals of the American Thoracic Society 2017, 14 (7), 1103–1107. DOI: 10.1513/AnnalsATS.201702-156PS. [PubMed: 28481631]
39. Meenach SA; Vogt FG; Anderson KW; Hilt JZ; McGarry RC; Mansour HM, Design, physicochemical characterization, and optimization of organic solution advanced spray-dried inhalable dipalmitoylphosphatidylcholine (DPPC) and dipalmitoylphosphatidylethanolamine poly(ethylene glycol) (DPPE-PEG) microparticles and nanoparticles for targeted respiratory nanomedicine delivery as dry powder inhalation aerosols. International journal of nanomedicine 2012, 8, 275–293.
40. Wang Z; Cuddigan JL; Gupta SK; Meenach SA, Nanocomposite microparticles (nCmP) for the delivery of tacrolimus in the treatment of pulmonary arterial hypertension. Int J Pharm 2016, 512 (1), 305–13. DOI: 10.1016/j.ijpharm.2016.08.047. [PubMed: 27568494]
41. Ren H; Birch NP; Suresh V, An Optimised Human Cell Culture Model for Alveolar Epithelial Transport. PloS one 2016, 11 (10), e0165225–e0165225. DOI: 10.1371/journal.pone.0165225. [PubMed: 27780255]
42. Gupta SK; Torrico Guzman EA; Meenach SA, Coadministration of a tumor-penetrating peptide improves the therapeutic efficacy of paclitaxel in a novel air-grown lung cancer 3D spheroid model. Int J Cancer 2017 DOI: 10.1002/ijc.30913.
43. Gillies ER; Goodwin AP; Fréchet JMJ, Acetals as pH-Sensitive Linkages for Drug Delivery. Bioconjugate Chemistry 2004, 15 (6), 1254–1263. DOI: 10.1021/bc049853x. [PubMed: 15546191]
44. Moore TL; Rodriguez-Lorenzo L; Hirsch V; Balog S; Urban D; Jud C; Rothen-Rutishauser B; Lattuada M; Petri-Fink A, Nanoparticle colloidal stability in cell culture media and impact on cellular interactions. Chem Soc Rev 2015, 44 (17), 6287–305. DOI: 10.1039/c4cs00487f. [PubMed: 26056687]
45. Kalaydina R-V; Bajwa K; Qorri B; Decarlo A; Szewczuk MR, Recent advances in “smart” delivery systems for extended drug release in cancer therapy. International journal of nanomedicine 2018, 13, 4727–4745. DOI: 10.2147/IJN.S168053. [PubMed: 30154657]

46. Karner S; Anne Urbanetz N, The impact of electrostatic charge in pharmaceutical powders with specific focus on inhalation-powders. Journal of Aerosol Science 2011, 42 (6), 428–445. DOI: 10.1016/j.jaerosci.2011.02.010.
47. Koullapis PG; Kassinos SC; Bivolarova MP; Melikov AK, Particle deposition in a realistic geometry of the human conducting airways: Effects of inlet velocity profile, inhalation flowrate and electrostatic charge. Journal of Biomechanics 2016, 49 (11), 2201–2212. DOI: 10.1016/j.jbiomech.2015.11.029. [PubMed: 26806688]
48. Vehring R, Pharmaceutical particle engineering via spray drying. Pharmaceutical Research 2008, 25 (5), 999–1022. DOI: 10.1007/s11095-007-9475-1. [PubMed: 18040761]
49. Win KY; Feng SS, Effects of particle size and surface coating on cellular uptake of polymeric nanoparticles for oral delivery of anticancer drugs. Biomaterials 2005, 26 (15), 2713–22. DOI: 10.1016/j.biomaterials.2004.07.050. [PubMed: 15585275]
50. Salomon JJ; Muchitsch VE; Gausterer JC; Schwagerus E; Huwer H; Daum N; Lehr C-M; Ehrhardt C, The Cell Line NCl-H441 Is a Useful in Vitro Model for Transport Studies of Human Distal Lung Epithelial Barrier. Molecular Pharmaceutics 2014, 11 (3), 995–1006. DOI: 10.1021/mp4006535. [PubMed: 24524365]
51. Galmarini CM; Tannock IF; Patel K; Trédan O, Drug Resistance and the Solid Tumor Microenvironment. JNCI: Journal of the National Cancer Institute 2007, 99 (19), 1441–1454. DOI: 10.1093/jnci/djm135. [PubMed: 17895480]
52. Lv D; Hu Z; Lu L; Lu H; Xu X, Three-dimensional cell culture: A powerful tool in tumor research and drug discovery. Oncology letters 2017, 14 (6), 6999–7010. DOI: 10.3892/ol.2017.7134. [PubMed: 29344128]
53. Stylianopoulos T; Munn LL; Jain RK, Reengineering the Physical Microenvironment of Tumors to Improve Drug Delivery and Efficacy: From Mathematical Modeling to Bench to Bedside. Trends in Cancer 2018, 4 (4), 292–319. DOI: 10.1016/j.trecan.2018.02.005. [PubMed: 29606314]
54. Tannock IF; Lee CM; Tunggal JK; Cowan DSM; Egorin MJ, Limited Penetration of Anticancer Drugs through Tumor Tissue. Clinical Cancer Research 2002, 8 (3), 878. [PubMed: 11895922]
55. Ramanujan S; Pluen A; McKee TD; Brown EB; Boucher Y; Jain RK, Diffusion and convection in collagen gels: implications for transport in the tumor interstitium. Biophysical journal 2002, 83 (3), 1650–1660. DOI: 10.1016/S0006-3495(02)73933-7. [PubMed: 12202388]
56. Liu F; Haeger CM; Dieffenbach PB; Sicard D; Chrobak I; Coronata AMF; Velandia MMS; Vitali S; Colas RA; Norris PC; Marinković A; Liu X; Ma J; Rose CD; Lee S-J; Comhair SAA; Erzurum SC; McDonald JD; Serhan CN; Walsh SR; Tschumperlin DJ; Fredenburgh LE, Distal vessel stiffening is an early and pivotal mechanobiological regulator of vascular remodeling and pulmonary hypertension. JCI Insight 2016, 1 (8). DOI: 10.1172/jci.insight.86987.

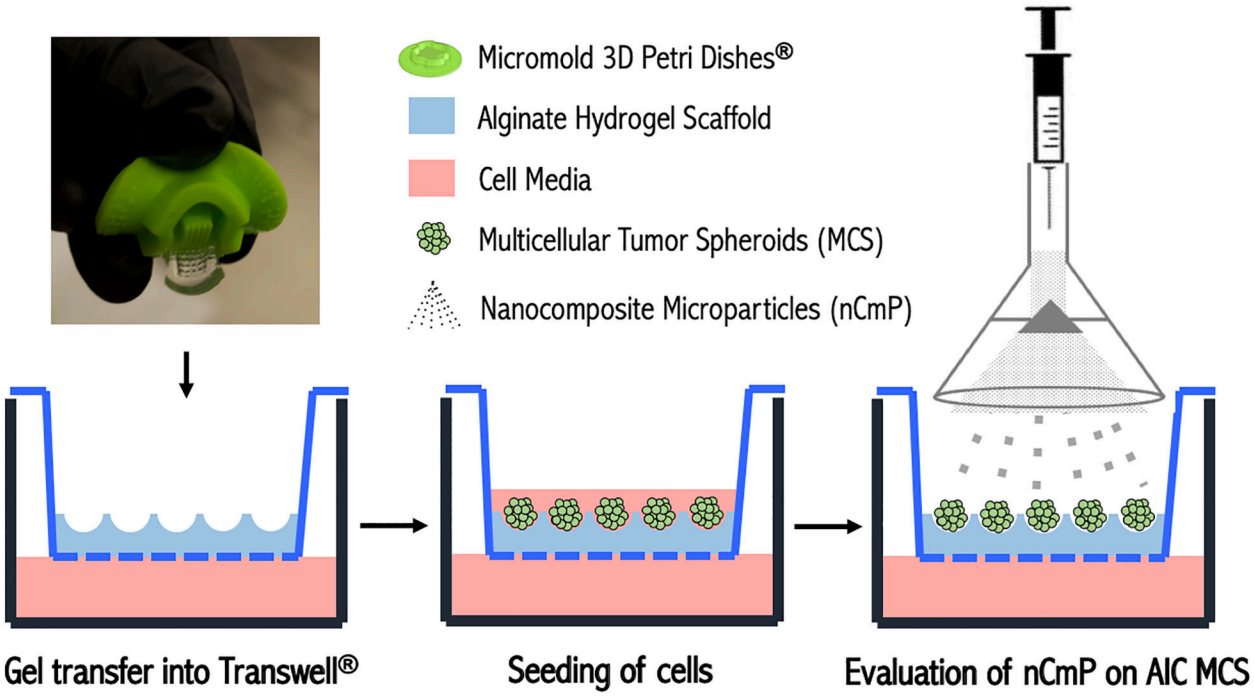


**Figure 1.**

Schematic of the formation of three-dimensional (3D) multicellular tumor spheroids (MCS) on an alginate scaffold in an 3D air interface culture (AIC) platform followed by exposure to aerosolized nanocomposite microparticles (nCmP).

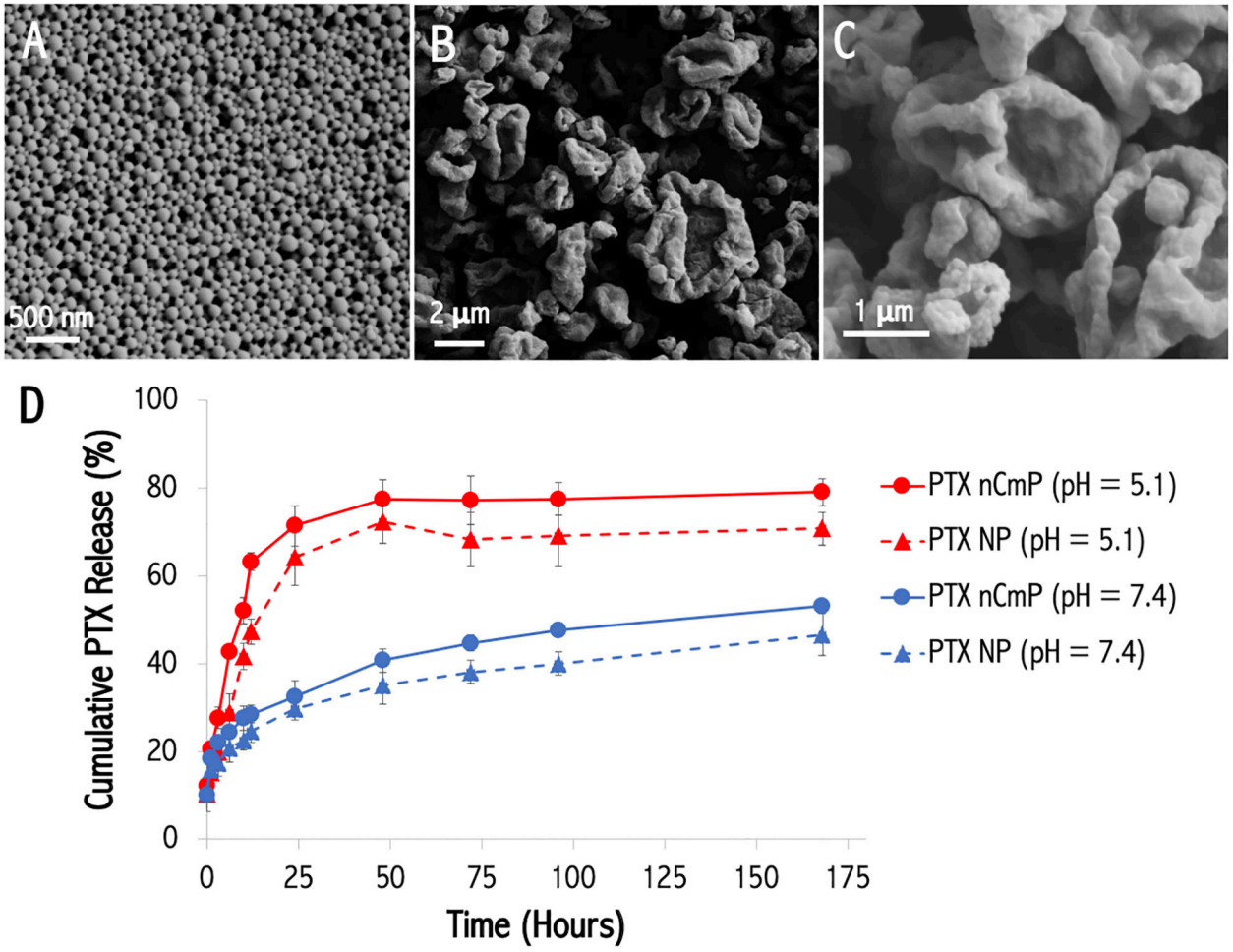


**Figure 2.**

Representative scanning electron micrographs of nanoparticles (NP) and nanocomposite microparticles (nCmP) systems, and their *in vitro* paclitaxel (PTX) release profiles at different pH values. (A) paclitaxel-loaded nanoparticles (PTX NP) at 20,000X, (B) paclitaxel nanocomposite microparticles (PTX nCmP) at 5,000X, and (C) PTX nCmP at 40,000X. (D) Comparative release profiles of PTX from PTX NP and PTX nCmP at pH 7.4 and pH 5.1 (n = 3).

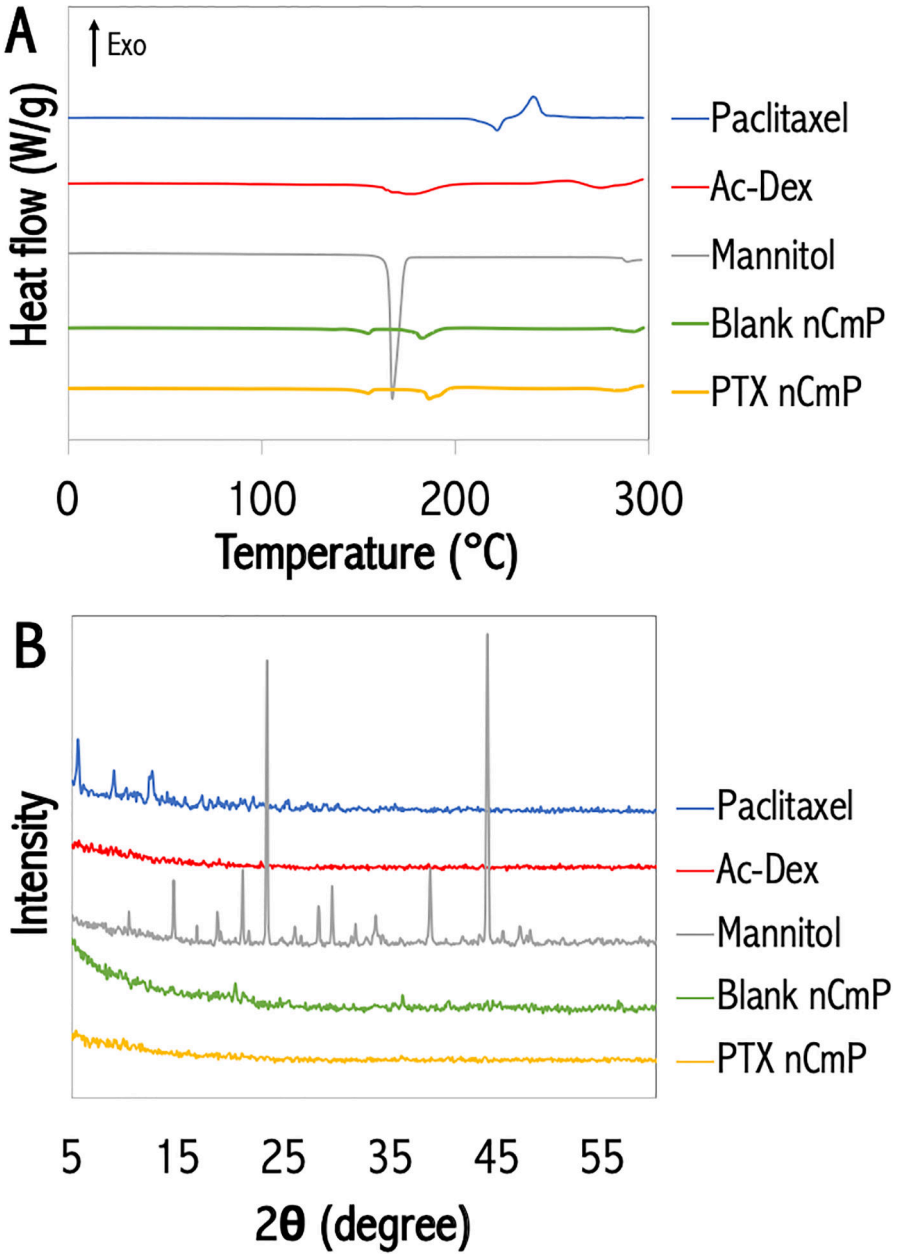


**Figure 3.**

(A) Differential scanning calorimetry (DSC) thermograms and (B) powder X-ray diffractograms (PXRD) of raw paclitaxel (Paclitaxel), raw acetalated dextran (Ac-Dex), raw mannitol (Mannitol), blank nanocomposite microparticles (Blank nCmP) and paclitaxel-loaded nCmP (PTX nCmP).

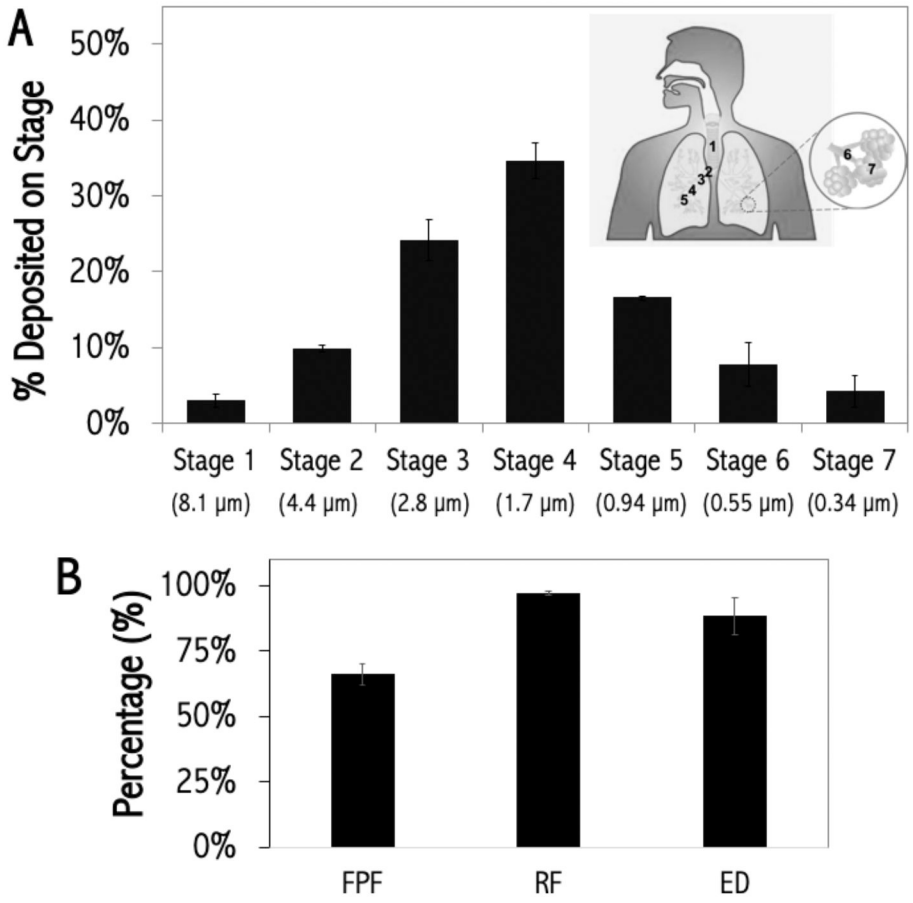


**Figure 4.**

*In vitro* aerosol dispersion performance of paclitaxel-loaded nanocomposite microparticles (PTX nCmP) in a Next Generation Impactor™ (NGI™) for Q = 60 L/min. (A) Particle deposition on each stage of the NGI, including the particle size cutoff corresponing to every stage (µm), (B) fine particle fraction (FPF), respirable fraction (RF), and emitted dose (ED) of PTX nCmP (mean ± standard deviation, n=3).

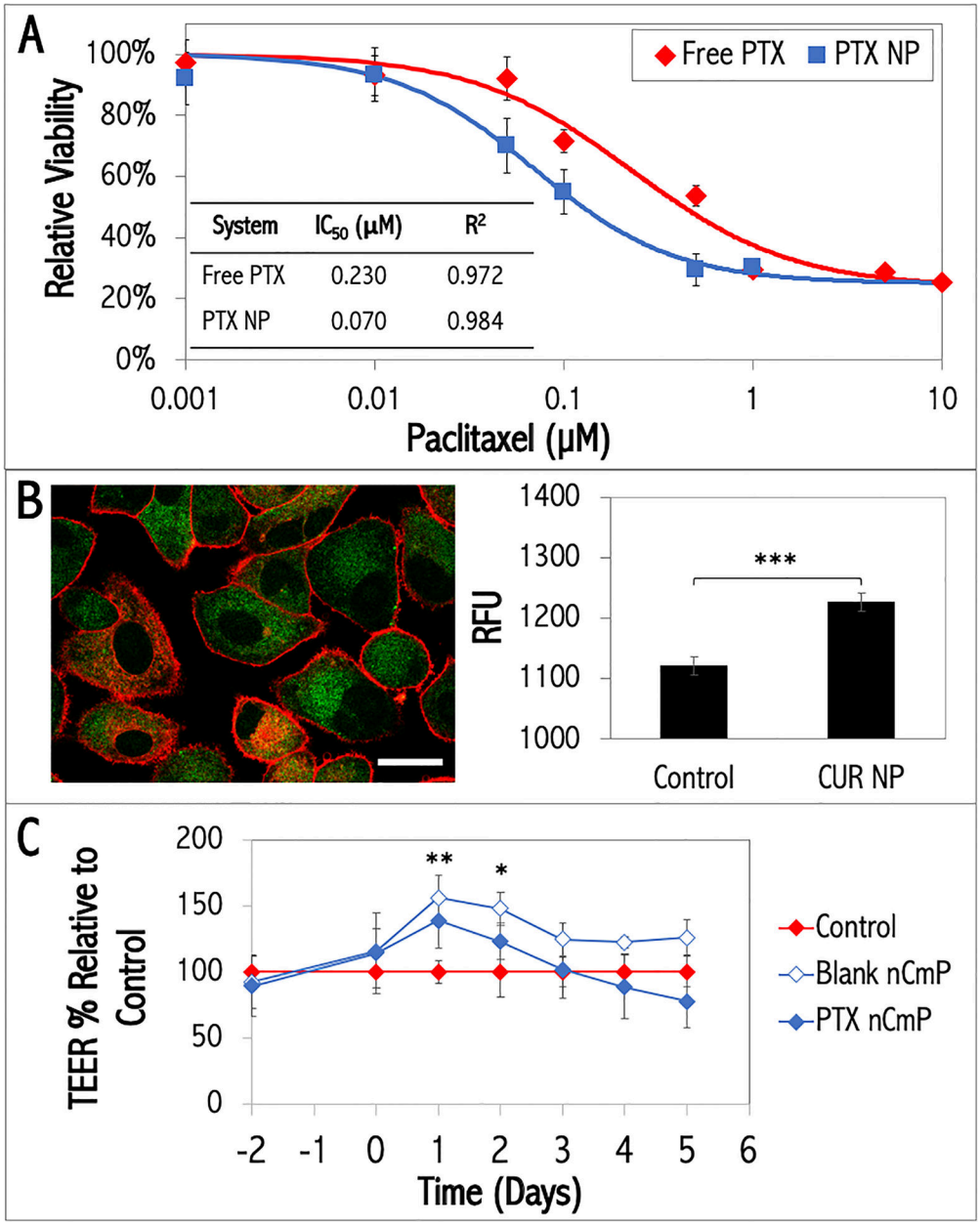


**Figure 5.**

Two-dimensional (2D) cell culture evaluations including: (A) Cell viability and $IC_{50}$ values of A549 cells dosed with free paclitaxel (PTX) and paclitaxel-loaded NP (PTX NP) for 48 hours. (B) Cellular uptake of fluorescent curcumin-loaded nanoparticles (CUR NP) in A549 cells following 3 hours of incubation, including (Left) a representative confocal image showing CUR NP (green) and cell membrane (red), scale bar = 20 μm and (Right) fluorescence quantification of uptake. (C) Transepithelial electrical resistance (TEER) analysis performed on H441 cells in air interface culture (AIC) condition after exposure to blank and paclitaxel-loaded nanocomposite microparticles (Blank nCmP and PTX nCmP, respectively). Statistical analysis was performed using Student's t-test, where * $p < 0.05$, **

$p < 0.01$, *** $p < 0.001$; $n \geq 3$, which represents the comparison to control (cells in media only).

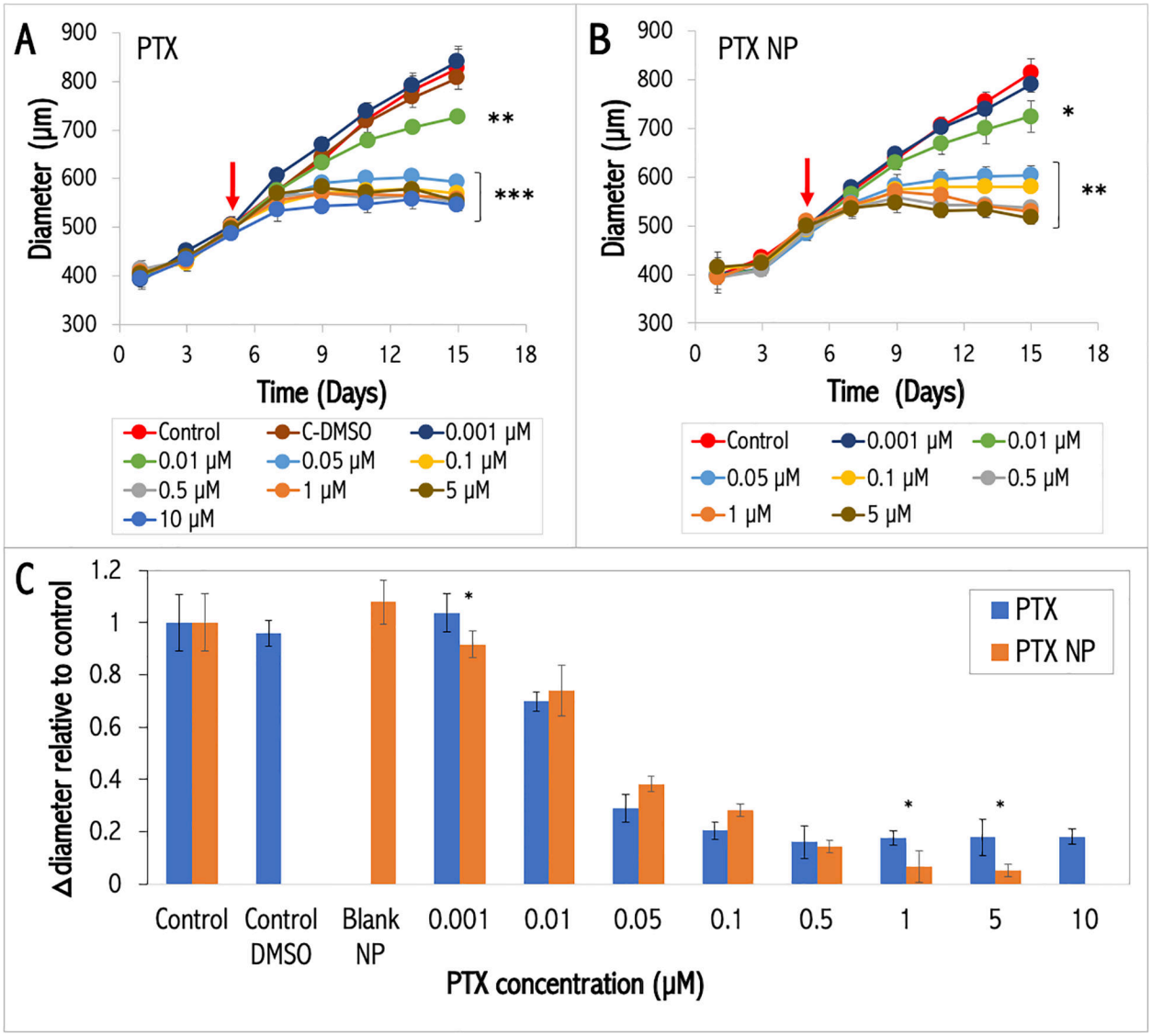


**Figure 6.**

Analysis of three-dimensional (3D) A549 multicellular spheroid (MCS) growth in liquid culture conditions upon exposure to different concentrations of paclitaxel (PTX) formulations, including: (A) free PTX and (B) PTX NP. (C) Comparison of the change in diameter relative to control (media only) upon exposure to free PTX and PTX NP at day 15. The red arrows indicate when the MCS were dosed with PTX or PTX NP. Statistical analysis was performed using Student's t-test, where * $p < 0.05$, ** $p < 0.01$, *** $p < 0.001$ to compare PTX versus PTX NP; $n \geq 3$.

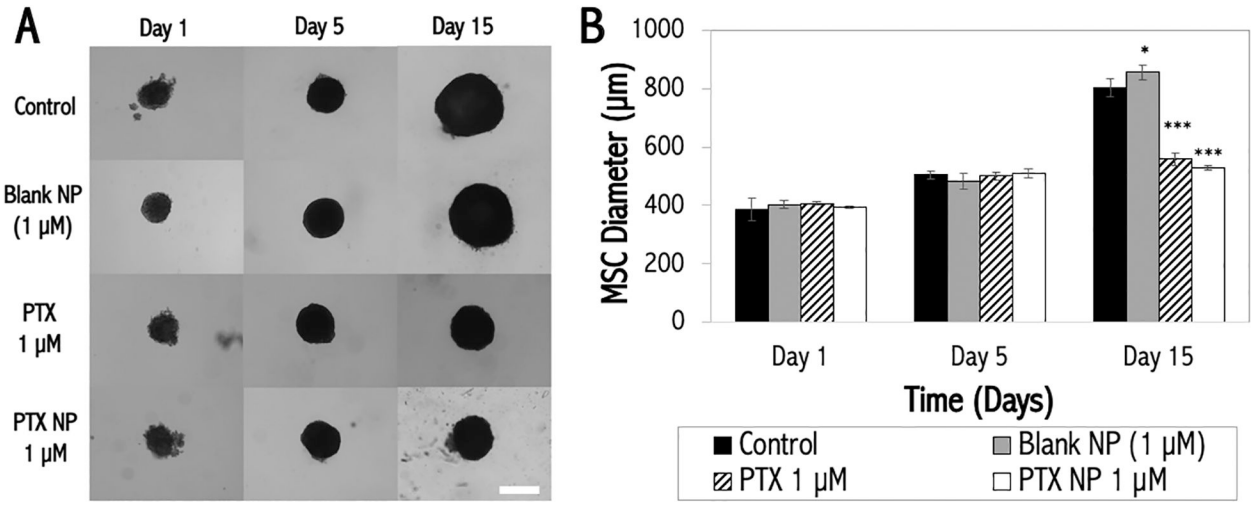


**Figure 7.**

(A) Representative bright-field images (scale bar = 500 μm), and (B) corresponding quantification of A549 three-dimensional (3D) multicellular spheroid (MCS) growth in liquid culture conditions upon exposure to 1 μM of free PTX, PTX nanoparticles (NP), and Blank NP equivalent to 1 μM of NP (by mass). Control MCS were exposed to media only. Statistical analysis was performed using Student's t-test, where * $p < 0.05$, ** $p < 0.01$, *** $p < 0.001$; $n \geq 3$, which represents the comparison to control (no exposure to PTX or NP).

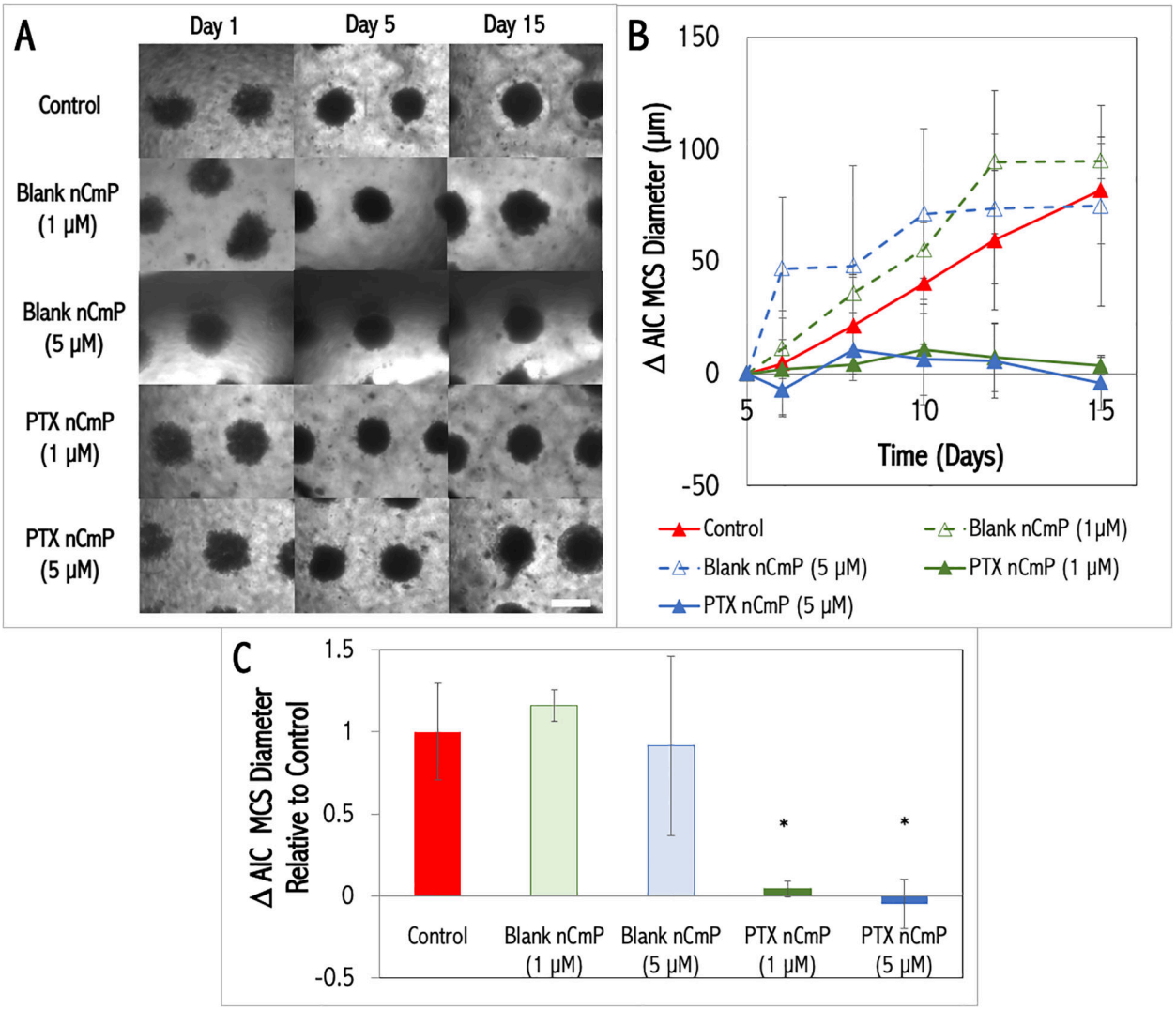


**Figure 8.**

Analysis of three-dimensional (3D) A549 multicellular spheroids (MCS) growth in air interface culture (AIC) conditions upon exposure to aerosolized paclitaxel-loaded nanocomposite microparticles (PTX nCmP). (A) Representative bright-field images of AIC MCS exposed to Blank nCmP and PTX nCmP (equivalent to 1 μM and 5 μM of PTX by mass used in liquid covered culture studies), scale bar = 500 μm. (B) Change in diameter of AIC MCS exposed to Blank and PTX nCmP over time compared to control. (C) Comparison of the change in AIC MCS diameters relative to control upon exposure to Blank and PTX nCmP at day 15. Statistical analysis was performed using Student's t-test, where * $p < 0.05$, $n \geq 3$; which represents the comparison to control (AIC MCS only).

**Table 1.**

Characteristics of paclitaxel (PTX)-loaded nanoparticles (NP), blank NP without PTX, PTX NP re-dispersed from PTX nanocomposite microparticles, and curcumin (CUR)-loaded NP. Analysis includes NP diameter as measured by dynamic light scattering (DLS) and ImageJ, polydispersity index (PDI), zeta (ζ) potential, PTX loading in NP, and encapsulation efficiency (EE) (mean ± standard deviation, n = 3).

| Particle System | Method | Diameter (nm) | PDI | ζ Potential (mV) | PTX Loading (μg PTX/mg NP) | EE (%) |
|---|---|---|---|---|---|---|
| PTX NP | DLS | 198.4 ± 9.9 | 0.14 ± 0.04 | −3.14 ± 0.55 | 35.73 ± 1.56 | 71.46 ± 3.11 |
| | ImageJ | 103.6 ± 19.3 | N/A | N/A | | |
| Blank NP | DLS | 191.9 ± 3.5 | 0.12 ± 0.02 | −4.79 ± 0.63 | N/A | N/A |
| | ImageJ | 150.3 ± 25.9 | N/A | N/A | | |
| Re-dispersed PTX NP | DLS | 270.7 ± 11.0 | 0.34 ± 0.03 | −18.47 ± 0.42 | N/A | N/A |
| CUR NP | DLS | 182.10 ± 2.04 | 0.11 ± 0.03 | −4.08 ± 0.25 | 14.73 ± 0.11 * | N/A |

* μg CUR/mg NP

**Table 2.**

Characteristics of paclitaxel (PTX)-loaded nanocomposite microparticles (nCmP), including water content, PTX loading, nanoparticle (NP) loading in nCmP, NP loading efficacy in nCmP, geometric diameter (via Image J), tapped density, theoretical mass median aerodynamic diameter ($MMAD_T$), experimental MMAD ($MMAD_E$), and geometric standard deviation (GSD) (mean ± standard deviation, n=3).

| Particle System | Water Content (%) | PTX Loading (μg PTX/mg nCmP) | NP Loading in nCmP (%) | NP Loading Efficacy in nCmP (%) |
|---|---|---|---|---|
| PTX nCmP | 2.78 ± 0.50 | 30.38 ± 0.80 | 85.01 ± 2.24 | 106.27 ± 2.80 |

| Particle System | Geometric diameter (μm) | Tapped Density ($g/cm^3$) | $MMAD_T$ (μm) | $MMAD_E$ (μm) | GSD (μm) |
|---|---|---|---|---|---|
| PTX nCmP | 2.17 ± 0.59 | 0.33 ± 0.01 | 1.25 ± 0.01 | 2.44 ± 0.25 | 2.34 ± 0.42 |